

The Influence of Wind Direction on Campbell Scientific CSAT3 and Gill R3-50 Sonic Anemometer Measurements

LAURENT GRARE, LUC LENAIN, AND W. KENDALL MELVILLE

Scripps Institution of Oceanography, University of California, San Diego, La Jolla, California

(Manuscript received 1 March 2016, in final form 22 July 2016)

ABSTRACT

Measurements from the Campbell CSAT3 and Gill R3-50 anemometers were conducted in four different experiments, in laboratory and field environments. Consistent differences between these two sonic anemometers were observed. The data have revealed that the differences were strongly correlated with the wind direction. According to the datasets used, the CSAT3 was the anemometer whose measurements were more sensitive to the instrument's orientation relative to the wind direction. While the mean wind speed and direction remained within the manufacturers' specifications (a few percent for the wind speed and a few degrees for the wind direction), the estimates of the friction velocity from the CSAT3 differed from the R3-50 by up to 20%.

1. Introduction

Three-dimensional sonic anemometer–thermometers are high-temporal-resolution instruments, commonly used in micrometeorological studies to sample atmospheric turbulence and to estimate fluxes of momentum and sensible heat. Measurements of these fluxes using eddy covariance techniques rely on the assumption that wind velocities and temperature are measured accurately. Several types of sonic anemometers are commercially available that mainly differ in their mechanical design. They are delivered with standard calibrations made by the manufacturer. Although sonic anemometers appear to retain their calibration over time quite well, the manufacturers do not provide detailed specifications on the accuracy of their instruments, especially regarding the covariance terms.

A wind tunnel study by [Grelle and Lindroth \(1994\)](#) has shown that some sonic anemometer outputs vary strongly with azimuth and elevation angles due to the complicated 3D interaction between the flow and the instrument itself. It was found that it is possible to construct an individual 3D calibration matrix for each instrument, the

application of which results in an appreciable reduction of the calibration error. However, although this result is strictly applicable in laminar stationary wind tunnel flows, it has been generally assumed that the result is valid also when the instrument is subjected to natural turbulent winds. This assumption has been criticized by [Hogstrom and Smedman \(2004\)](#), who have shown that the application of the 3D calibration matrix in the field does not guarantee a proper reduction of the calibration error.

Several intercomparison experiments ([Loescher et al. 2005](#); [Mauder et al. 2007](#)) have been conducted to evaluate the differences between sonic anemometers (including the Campbell Scientific CSAT3 3D sonic anemometer and an earlier release of the Gill R3-50 three-axis ultrasonic anemometer) in their estimation of the mean wind speed, the variances of the wind and temperature components, and their estimation of the momentum and sensible heat fluxes. These studies have shown that the relative errors between instruments in the estimate of the momentum and sensible heat fluxes are up to 10%–15%, depending on the instruments considered.

In recent years, ultrasonic anemometers have been shown to suffer errors due to the angle of attack, which is the angle between the wind vector and the horizontal. Several studies ([van der Molen et al. 2004](#); [Nakai et al. 2006](#); [Nakai and Shimoyama 2012](#); [Nakai et al. 2014](#)) have been performed both in wind tunnels and in the field to quantify and correct these errors for Gill sonic anemometers (Solent R2 and R3, WindMaster). In addition,

 Denotes Open Access content.

Corresponding author address: Laurent Grare, Scripps Institution of Oceanography, UCSD, 9500 Gilman Dr., La Jolla, CA 92093-0213.

E-mail: lgrare@ucsd.edu

DOI: 10.1175/JTECH-D-16-0055.1

Meyers and Heuer (2006) reported that angle-of-attack errors exist using model 81000 ultrasonic anemometers (R. M. Young, Traverse, Michigan). This suggests that these errors occur not only for Gill sonic anemometers but also for sonic anemometers from other manufacturers. These studies showed that the vertical wind velocity component was substantially underestimated by these anemometers, especially at a large angle of attack, and that the horizontal velocity component was also sensitive to the angle of attack and the wind direction. They showed that these errors can lead to an underestimation of the momentum and sensible heat fluxes by 10%–20%.

Recently, Kochendorfer et al. (2012) and Frank et al. (2013) have compared sonic anemometers with orthogonal (SATI/3Vx, Applied Technologies, Inc.) and non-orthogonal transducers (CSAT3, R. M. Young). They found that nonorthogonal sonic anemometers underestimate the vertical wind speed by about 10%, leading to an underestimation of the fluxes by the same order of magnitude. Nevertheless, Mauder (2013) criticized these results, claiming that the underestimation was less than a few percent.

Over the last couple of years, Campbell Scientific, Inc. has openly disclosed that the CSAT3 anemometers were not corrected for the transducer's shadowing effects. Following the release of this information, Horst et al. (2015) and Frank et al. (2016) discussed the pertinence of the Kaimal (1978) correction for the shadowing of the transducers in CSAT3 measurements. While both authors showed that this correction was able to narrow the gap between statistical measures of the wind components observed between orthogonal and nonorthogonal sonic anemometers, there is still no consensus on the best way to fix the CSAT3 for these transducer shadowing effects.

More recently, Gill has announced that there was an internal firmware bug that caused an underestimation of the vertical component with the WindMaster and WindMaster Pro models. This bug has been fixed in the latest firmware that they released. However, this bug did not affect the models R3, HS, R3-50, and HS-50. This last statement meant that the correction proposed by Nakai and Shimoyama (2012) was applicable only to the WindMaster and WindMaster Pro models.

The previous studies have mostly focused on discrepancies between instruments, highlighting the influence of errors due to large angles of attack for some anemometers. Although authors have suggested that some errors can be associated with the wind direction, not much has been done to study the effects of the wind direction on the accuracy of sonic anemometers, especially at small angles of attack.

Here we conducted field measurements using Campbell CSAT3 and Gill R3-50 sonic anemometers over ocean

waves that have highlighted the influence of the wind direction on the discrepancies we observed between the two types of anemometers. Additional measurements both in the field and in a wind tunnel have confirmed that the wind direction was the main parameter controlling the observed discrepancies between the two instruments.

In this paper, we present results from these four datasets that describe the influence of the wind direction on the accuracy of several variables measured by these two sonic anemometers. In section 2, we present the instruments, the experimental design of the four experiments, and the methods used to process the data. Results are presented in section 3 and are discussed in section 4 before the conclusions in section 5. In the appendix, we compare the data presented in the main body of the paper to CSAT3 data corrected for the shadowing of the transducers following the method described recently in Horst et al. (2015).

2. Methods

a. Sonic anemometers

The datasets presented in this paper were collected during four distinct experiments using the same CSAT3 and Gill sonic anemometers. For all four of these experiments, the CSAT3 and the Gill were mounted vertically and their relative azimuthal orientation remained the same. The Gill anemometer was oriented such that the rods of its cage were symmetric around the vertical plane defined by the CSAT3 body; that is, when the CSAT3 was aligned with and facing the wind, two of the three rods of the Gill's cage were oriented at $\pm 60^\circ$ from the wind direction, while the third rod was downwind of the volume of measurement (see Fig. 1). According to the frames defined in the CSAT3 and the Gill manuals (Campbell Scientific, Inc. 2015; Gill Instruments Ltd. 2005), the x axis of the CSAT3 was aligned with the north axis of the Gill. The azimuth angle Ψ between the wind and the instruments is defined as follows:

$$\Psi = \arctan(U_y/U_x), \quad (1)$$

where U_x and U_y are the mean along and cross components of the wind, respectively, in the frame of the anemometer.

b. The experiments

1) SOCAL 2013

The first dataset was collected during the Office of Naval Research Southern California 2013 (SoCal2013) experiment. This experiment was conducted on the Research Platform (R/P) *Floating Instrument Platform*

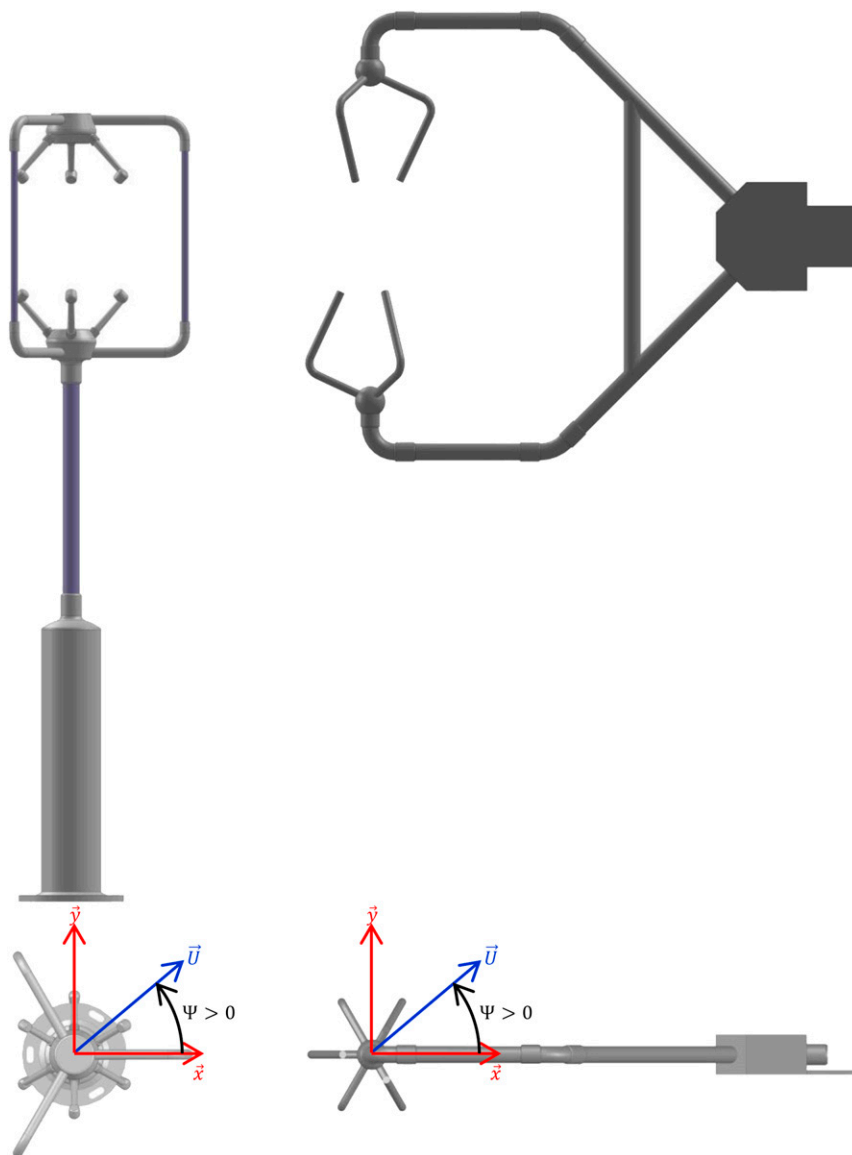


FIG. 1. The (right) CSAT3 and (left) Gill R3-50 3D sonic anemometers, their axes of reference, and the definition of the azimuthal angle of the wind Ψ .

(*FLIP*) off the coast of Southern California from 7 to 22 November 2013. The R/P *FLIP* is a 108-m-long open ocean research platform designed to be partially flooded in order to flip to a vertical position. When flipped, the R/P *FLIP* is very stable because it is mostly immune to the effects of the waves. Furthermore, 18-m-long booms are deployed on the starboard, port, and deck side of the hull, allowing the mounting of instruments away from flow distortion due to the hull of *FLIP*. During this experiment, five sonic anemometers (four CSAT3 and one Gill R3-50) were mounted on a vertical telescopic mast that was deployed from the end of the port boom of *FLIP*. When the mast was fully extended, the anemometers

were vertically distributed from 15 down to 2.65 m above mean sea level (MSL). The purpose of this setup was to measure at the same time the friction velocity at different levels and the vertical mean wind profile in order to assess the validity of the logarithmic wind profile above waves and to determine how the wind stress extrapolated from the wind speed profile compared to the wind stress directly measured with the eddy covariance method. It turned out that there were significant differences between measurements from the CSAT3s and the Gill anemometer, differences that were primarily related to the wind direction. These initial results led to the experiments presented below in order to evaluate the

consequences of these differences between the two most widely used sonic anemometers for flux measurements. Therefore, the data gathered during the SoCAL2013 experiment should not be interpreted as being the best dataset to assess the differences between these two anemometers, but the results from this dataset should rather be treated as the initial pieces of evidence showing the great influence of the wind direction in the discrepancies observed between the CSAT3s and the Gill anemometer. Four CSAT3s and one Gill anemometer were mounted on the mast but only data from the two lowest anemometers (one CSAT3 and the Gill) are presented in this paper. We decided to limit the comparison to these two anemometers because they were the closest to each other and their spatial separation remained constant throughout the entire experiment. The CSAT3 was located 0.85 m above and 1 m ahead of the Gill as shown in Fig. 2a. The height of the anemometers was adjusted depending on the wave conditions and remained in the range $3.5 < z < 5.95$ m for the CSAT3 ($2.65 < z < 5.1$ m for the Gill), where z is the height above the mean sea level. The wind speed ranged from 0 to 12 m s^{-1} . Datasets were motion compensated to account for the motion of *FLIP* and the mast following Edson et al. (1998), using measurements from an inertial measurement unit (IMU) mounted close to the anemometers (see dimensions in green in Fig. 2a). For most of the experiment, the wind was coming from a direction to the right of the anemometers, that is, with Ψ in the range $[0^\circ; +60^\circ]$. This dataset is composed of an ensemble of 560×30 min records from which statistical variables were computed.

2) SIO PIER

The second dataset was collected from 5 August to 30 September 2014. The two sonic anemometers were mounted at the end of a 5-m boom on the northwest corner of the Scripps Institution of Oceanography (SIO) pier, La Jolla, California. Their height above the mean sea level fluctuated between 10.4 and 12.8 m, depending on the tides. The two anemometers were separated laterally by 35 cm and the Gill was about 25 cm ahead of the CSAT3 (see dimensions in red in Fig. 2b). Cases such that $\Psi < -80^\circ$ and $\Psi > 80^\circ$ were excluded from the dataset so that measurements from one anemometer were not affected by the wake of the upwind anemometer. This dataset is composed of an ensemble of 2330×30 minute records from which statistical variables were computed.

3) TERRESTRIAL BOUNDARY LAYER

The terrestrial boundary layer (TBL) experiment was designed to gather data in moderate to high wind

conditions ($10\text{--}15 \text{ m s}^{-1}$). To achieve this goal, the telescopic mast that was used during the SoCal2013 experiment was adapted to be mounted on the back of a van in order to perform measurements in windy environments. The dataset presented in this paper was gathered on 3 September 2015, in the San Geronio Pass in California. We selected this pass because it is one of the windiest places in Southern California.¹ The van was located in an open area beside Railroad Avenue at the following location: $33^\circ 55' 21.85'' \text{N}$, $116^\circ 41' 24.79'' \text{W}$. When the mast was deployed, the two anemometers were mounted on a frame attached to the top of the mast (see Figs. 2c,d). With this setup, we were able to change the wind direction relative to the instruments by changing the orientation of the van while keeping the instruments at the same location. The elevation of the anemometers was approximately 10 m above ground, and they were 1 m apart. To control the horizontal displacements of the anemometers, the mast was rigged with lines attached to horizontal poles mounted on the front side of the van roof. Two XSENS inertial motion units were mounted as close as possible to the anemometers (see dimensions in green in Fig. 2d) to monitor their displacements, and to correct the wind measurements accordingly. During the deployment, the mean wind speed varied from 9 to 15 m s^{-1} , and we recorded twelve 20-min time series at different relative wind directions in the range $[-75^\circ; +75^\circ]$.

4) SDSU WIND TUNNEL

An additional dataset was collected in the San Diego State University (SDSU) wind tunnel. Each anemometer was tested in that tunnel at different wind speeds and at different orientations (Figs. 2e,f). The test section was 0.8 m high and 1.15 m wide. A Pitot tube connected to a differential pressure transducer (model 202BG, Paroscientific) was mounted 7 cm behind and 3 cm beside the measuring volume of the sonic anemometers. The experimental setup ensured that the location of the measuring volume remained the same regardless of the orientation of the instruments. The orientation of the instruments was adjusted by 15° increments from -60° to $+60^\circ$, as the wind tunnel was not wide enough to rotate the CSAT3 up to 90° . For these tests, the wind speed ranged from 2.8 to 20.7 m s^{-1} and the airflow was quasi laminar. To conduct the Pitot measurements when either the CSAT3 or the Gill was aligned with the wind (aligned and centered in the wind tunnel), the Pitot tube

¹ Incidentally, the San Geronio Pass Wind Farm, located on the eastern slope of the San Geronio Pass, is one of three major wind farms in California.

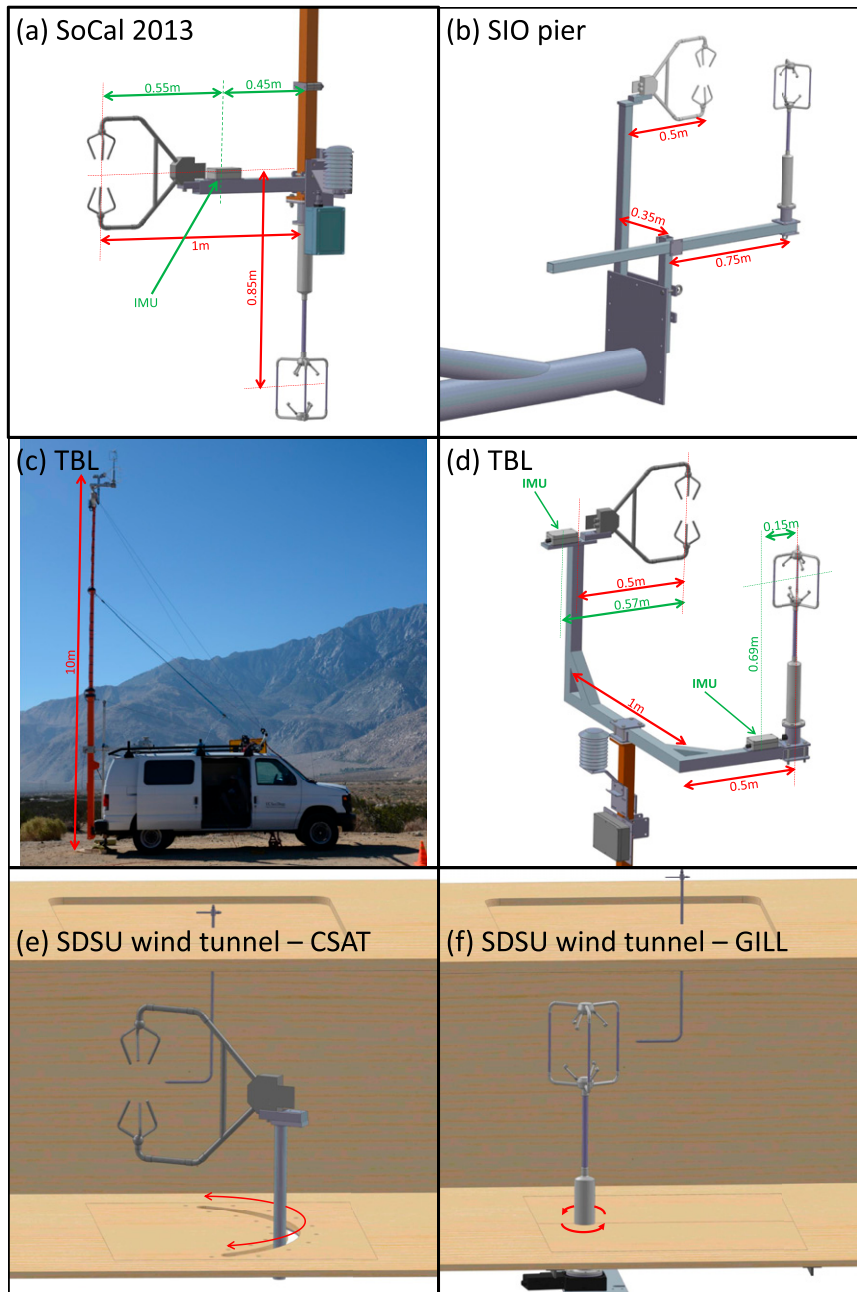


FIG. 2. Experimental setups for the four experiments: (a) SoCal 2013; (b) SIO pier test; (c),(d) TBL; and (e),(f) SDSU wind tunnel.

was not exactly centered laterally in the wind tunnel but was mounted 3 cm to the side. In this configuration, the anemometers did not wind shadow the Pitot tube when their orientation was within the range $\pm 60^\circ$. For larger angles, one of the rods of the cage of the Gill was upstream of the Pitot tube and created a wake responsible for abnormal low values of the mean wind speed measured by the Pitot tube. Therefore, data from the SDSU

wind tunnel are presented only for wind directions within the range $\pm 60^\circ$.

c. Data analysis

For all experiments, time series were recorded at 20 Hz on a CR3000 datalogger (Campbell Scientific, Inc., Logan, Utah). Both anemometers were sampled using their digital outputs and the Gill was configured to

output manufacturer-calibrated data. The field datasets were processed by removing 30-min records with physically unrealistic measurements (mean, standard deviation, number of samples) following Vickers and Mahrt (1997). Only data with wind speeds larger than 1 m s^{-1} were considered in the analysis. For the wind tunnel data, for each orientation, the wind speed was increased every 2 min, and after stationarity was reached within the first minute, only the second minute of recorded data was used in the analysis.

For all datasets, wind components were expressed in the streamwise coordinate system using the double rotation method (see Wilczak et al. 2001). In this streamwise coordinate system, the mean vertical W and cross V components of the wind were equal to zero.

Finally, the zero-offset values from both anemometers were measured to be less than 2 cm s^{-1} prior to the experiments, and since their influence on the following analysis was negligible, our data were not corrected to account for these offsets.

When presented as a function of Ψ , data from the SoCal2013 and SIO pier experiments were bin averaged per 15° wind direction bins following

$$\langle X \rangle(\Psi_i) = \frac{1}{M} \sum^M X(\Psi), \quad \Psi \in [\Psi_i - 7.5; \Psi_i + 7.5], \quad (2)$$

where $\langle X \rangle(\Psi_i)$ is the ensemble bin-averaged value expressed at the wind direction bin Ψ_i of the variable X expressed at any wind direction Ψ inside the range $[\Psi_i - 7.5; \Psi_i + 7.5]$.

Following the statements from Gill and the online statement from Nakai (https://sites.google.com/site/micrometeorologist/software/AoA_correction) regarding the internal firmware bug, data from the Gill were not correct with the routine developed by Nakai and Shimoyama (2012). Regarding the CSAT3, since there is still no consensus that the Kaimal correction is the appropriate method to correct the CSAT3 for the transducer's shadowing effects, we decided to present the raw data in the core of the paper. However, all CSAT3 data have been processed using the correction proposed by Horst et al. (2015), and this corrected set of data has been compared to the CSAT3 and Gill raw datasets. Relevant figures of this comparison are presented in the appendix.

3. Results

a. Mean wind speed

Figure 3 presents the relative difference in the estimates of the mean wind speed between anemometers

as a function of Ψ and the mean wind speed U . The relative difference $\Delta U/U$ is defined as follows:

$$\Delta U/U = \frac{U_C - U_G}{U_A}, \quad (3a)$$

$$\Delta U/U = \frac{U_X - U_P}{U_P}, \quad (3b)$$

where Eq. (3a) was used for the SoCal2013, SIO pier, and TBL datasets, while Eq. (3b) was used for the wind tunnel data. In Eq. (3a), U_A is the average of the CSAT3 and Gill mean wind speeds, that is, $U_A = 0.5(U_C + U_G)$. Subscripts C , G , and P correspond to CSAT3, Gill, and Pitot, respectively, while subscript X corresponds to either CSAT3 or Gill.

For all the cases, Fig. 3 shows that there was a strong correlation between the relative differences and the wind direction (left panels), while the correlation with the wind speed was poor (right panels), although there was a slight correlation with the wind speed in the wind tunnel.

For the SoCal2013 experiment, the collapse of the data was remarkable. The relative difference between instruments varied smoothly from -4% to $+4\%$ as the wind veered right to left. For the SIO pier test, although the collapse of the data was not as good as for SoCal2013, there was a distinct symmetric pattern when the relative difference was plotted as function of the wind direction. While the two sonic anemometers were in close agreement when the wind direction was greater than $\pm 30^\circ$, the difference reaches -2% when the wind was aligned with the instruments and the CSAT3 measured a wind speed that was smaller than that of the Gill.

The data from the TBL experiment also show that the wind speed measured by the CSAT3 was up to 4% smaller than that measured by the Gill. As for the measurements collected at the SIO pier, the wind speeds recorded by the two anemometers were in a better agreement (less than 2% difference) when the wind direction veered to the left or to the right. Data from the wind tunnel suggest that the mean wind speed from the Gill was not affected by the wind direction, and that the mean wind speed values were in agreement with the Pitot tube values with less than a 1% difference. But for the CSAT3, the deviation from the Pitot measurements varied from -2% to $+2\%$ depending on the wind direction, with maxima at $\Psi = \pm 30^\circ$.

b. Mean wind direction

Figure 4 shows the absolute difference in the mean wind direction $\Delta\Psi$ as a function of the wind direction for the four experiments. For the field experiments, the absolute difference corresponds to the mean wind direction difference between the two sonics (i.e., $\Delta\Psi = \Psi_C - \Psi_G$),

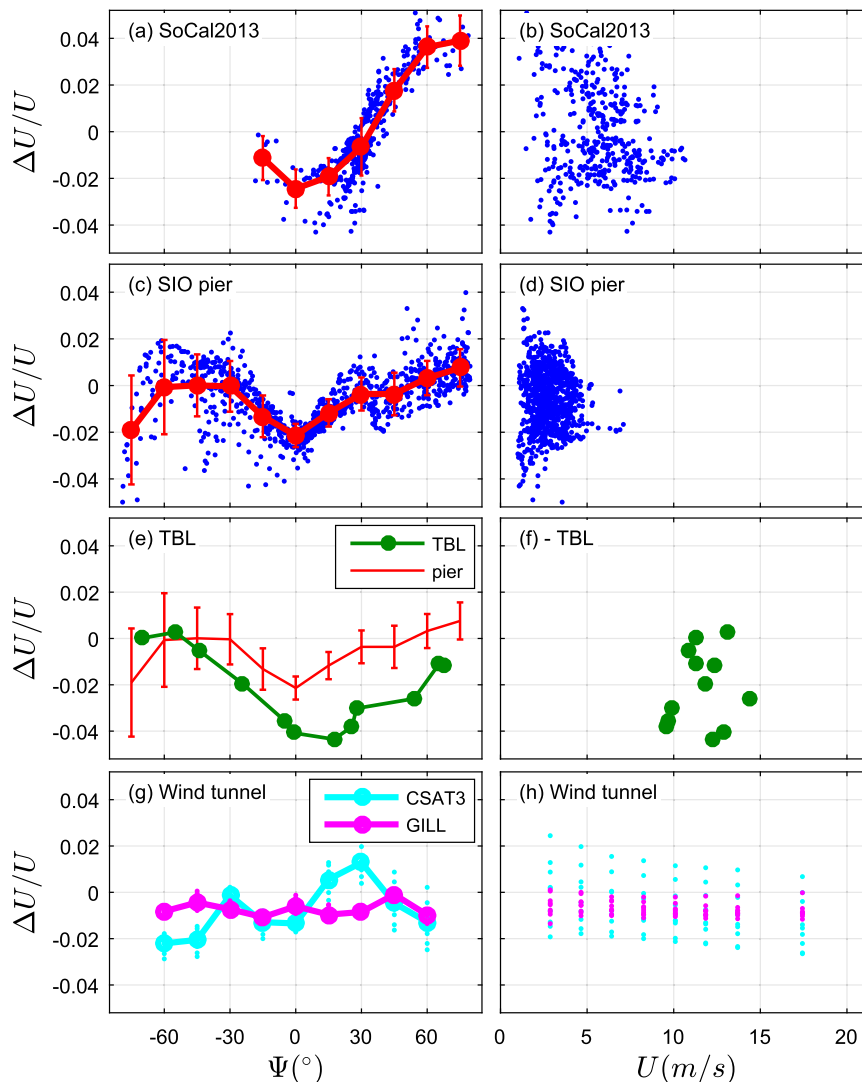


FIG. 3. Relative difference in the mean wind speed $\Delta U/U$ as a function of the (left) wind direction and (right) wind speed. See Eq. (3) for the definition of $\Delta U/U$. (a),(b) SoCal2013 experiment; (c),(d) SIO pier experiment; (e),(f) TBL experiment; and (g),(h), wind tunnel test. For the SoCal2013 and SIO pier experiments, each 30-min data point is reported with a blue point. The solid red circles joined by the thick red lines correspond to the averaged values in wind direction bins. The vertical error bars correspond to the standard deviation per 15° wind direction bin. For the TBL experiment, each 20-min-averaged data point is reported with a solid green circle. Bin-averaged values from the pier experiment are reported in (e) with a light red line. For the wind tunnel cases, the mean wind speed measured by each sonic is compared to the wind speed measured by the Pitot tube. Data from the CSAT3 are reported in cyan, while data from the Gill are reported in magenta.

while in the wind tunnel, $\Delta\Psi$ corresponds to the difference between the wind direction measured by the anemometer and the known angle of rotation of the instrument relative to the wind tunnel axis.

The data showed that in the wind tunnel, the Gill was not sensitive to the wind direction even when the rods of its cage were upstream of the volume of measurement (i.e., $\Psi = \pm 60^\circ$). But the data from the CSAT3

revealed a smooth and symmetric trend around $\Psi = 0^\circ$ with a 2° maximum deviation around $\pm 60^\circ$. This trend was comparable to the data from the SoCal2013 and TBL experiments and, to a lesser extent, comparable to the data from the pier. This suggests that the wind direction difference between the two sonic anemometers observed in the field experiments came primarily from errors in the CSAT3 measurements.

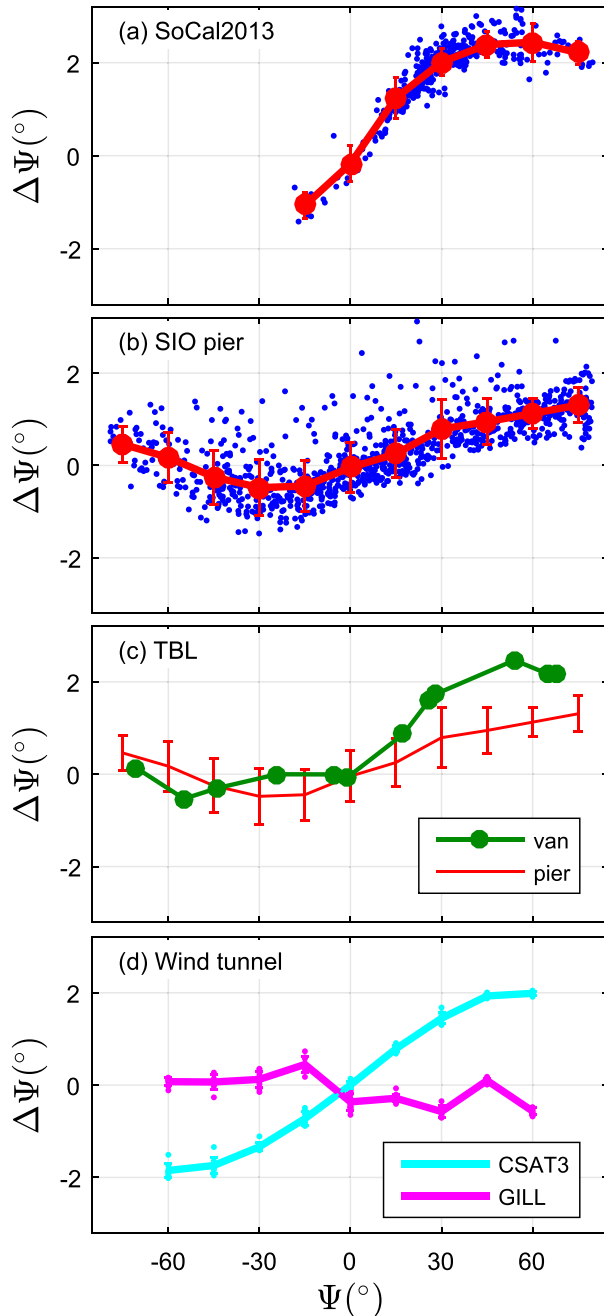


FIG. 4. Absolute difference in the wind direction $\Delta\Psi$ as a function of the wind direction. (a)–(c) For the field data, $\Delta\Psi = \Psi_C - \Psi_G$, where subscripts C and G refer to the CSAT3 and the Gill, respectively. (d) For the wind tunnel, $\Delta\Psi$ represents the difference between the wind direction measured by the instrument and the angle of rotation of the instrument. The shape and color of the points and lines are identical to those in Fig. 3.

c. Standard deviation of the vertical wind component

Figure 5 shows the relative difference in the standard deviation (σ_w) for the vertical component of the wind as a function of the wind direction for the field experiments.

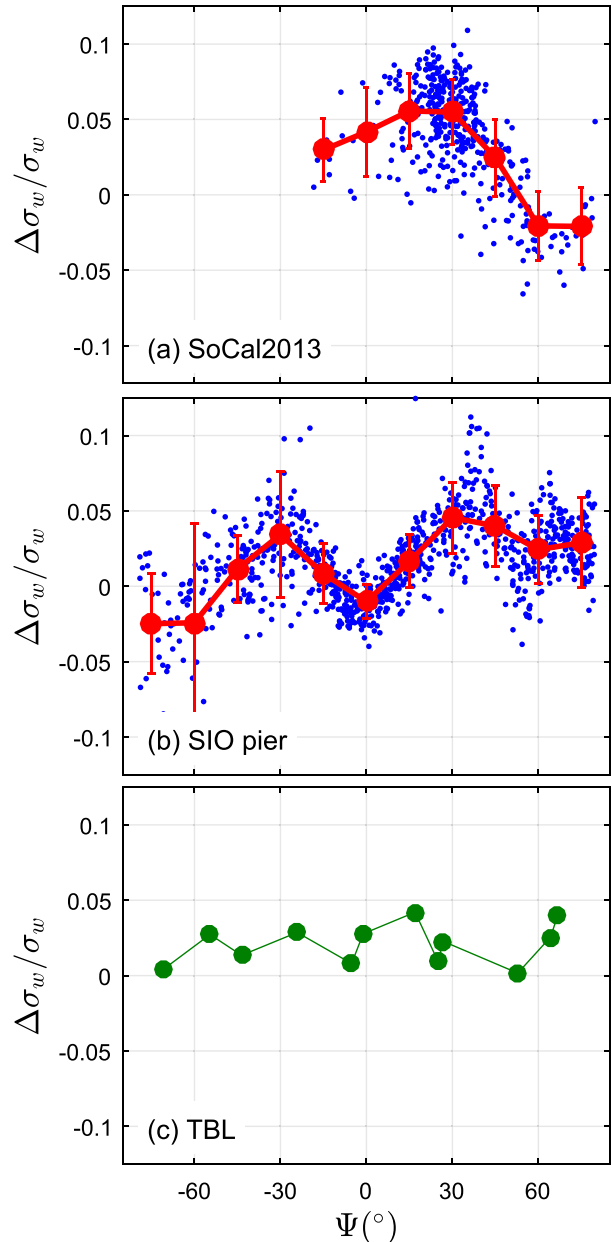


FIG. 5. Relative difference in σ_w as a function of the wind direction. The relative difference between the CSAT3 and the Gill data is $\Delta\sigma_w/\sigma_w = (\sigma_{wC} - \sigma_{wG})/\sigma_{wA}$, where the subscripts C and G refer to the CSAT3 and the Gill, respectively, and $\sigma_{wA} = 0.5(\sigma_{wC} + \sigma_{wG})$. For the SoCal2013 and SIO pier experiments, each 30-min average data point is reported with a blue point. The thick red lines correspond to the averaged values per 15° wind direction bin with their associated error bars, which correspond to the standard deviations for each wind direction bin. For the TBL experiment, the 20-min-averaged data points are plotted with solid green circles joined by a thin line.

As for the mean wind speed, the relative difference corresponds to the difference between the measurements from the CSAT3 σ_{wC} and measurements from the Gill σ_{wG} normalized by the average of the two anemometers,

$\sigma_{wA} = 0.5(\sigma_{wC} + \sigma_{wG})$. First, we need to emphasize that for the SoCal2013 experiment, the fact that the two anemometers were not located at the same height directly affected the comparisons. Indeed, close to surface waves, the fluctuations of the wind components (especially the vertical component) are strongly coupled to the waves and their amplitudes depend, at least, on the height above the water and the wave and the wind speeds. Therefore, no conclusions can be drawn from this experiment. For the SIO pier experiment, the collapse of the data was remarkable when plotted as a function of the wind direction. The shape of the bin-averaged data is quite comparable with the one observed in Fig. 3 for the mean wind speed. The relative difference reached its maximum (+5%) at both -30° and $+30^\circ$, while the two anemometers were in closer agreement when the wind was aligned with the instruments. For the TBL experiment, there was no significant variation associated with the wind direction. On average, all three experiments showed that the variance of w' measured by the CSAT3 is slightly larger than the one measured by the Gill.

d. Friction velocity and wind stress

We present in this section the influence of the wind direction on the friction velocity u_* , where

$$u_* = \sqrt{\overline{u'w'^2} + \overline{v'w'^2}}. \quad (4)$$

The covariances $\overline{u'w'}$ and $\overline{v'w'}$ were calculated for each 30-min (20 min for the TBL data) record from the integration of the cospectra $Co_{uw}(f)$ and $Co_{vw}(f)$ computed over 100-s sliding windows. The cospectra were integrated from the Nyquist frequency ($f_h = 10$ Hz) down to the lowest resolved frequency $f_l = 0.1$ Hz, for example,

$$\overline{u'w'} = \int_{f_l}^{f_h} Co_{uw}(\xi) d\xi. \quad (5)$$

Data from the wind tunnel are no longer presented in this section, since the flow was quasi laminar, and the values of u_* were not representative of a fully developed turbulent flow.

Figure 6 presents the relative difference in u_* as a function of the mean wind direction for the SoCal2013, SIO pier, and TBL experiments. As for the mean wind speed and the standard deviation of w' , the relative difference in u_* corresponds to the difference between instruments normalized by the average of the two instruments, that is, $\Delta u_*/u_* = (u_{*C} - u_{*G})/u_{*A}$. The figure shows that, for all cases, the relative difference reached a minimum when the wind was aligned with the instruments and that the relative difference increased

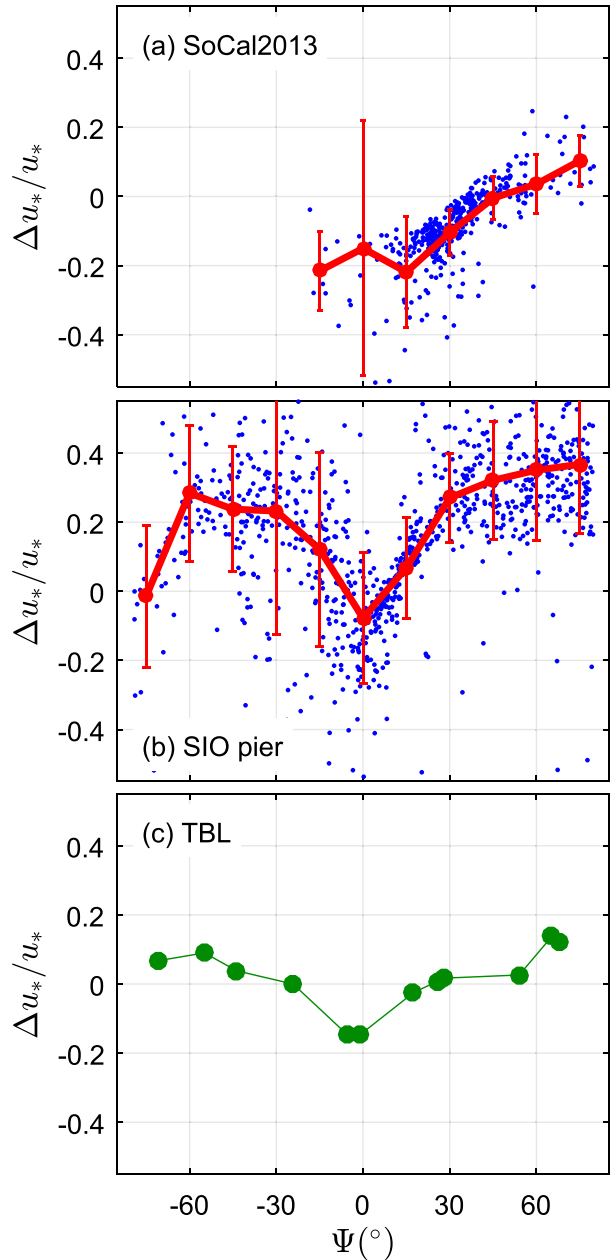


FIG. 6. Relative difference in the friction velocity u_* as a function of the wind direction. The relative difference corresponds to the deviation of the CSAT3 data from the Gill data, i.e., $\Delta u_*/u_* = (u_{*C} - u_{*G})/u_{*A}$, where the subscripts C and G refer to the CSAT3 and the Gill, respectively, and $u_{*A} = 0.5(u_{*C} + u_{*G})$. The shape and color of the points and lines are identical to those in Fig. 5.

when the wind veered to the left or to the right. While there were discrepancies between the different cases in the minimum and maximum values of $\Delta u_*/u_*$, the trends were similar, and the figure shows that the relative difference in u_* between the two anemometers

varied between -20% to $+20\%$ for strong winds (SoCal2013 and TBL tests), while the relative difference went up to $+40\%$ for lighter winds (SIO pier case).

Figure 7 shows the variation of the wind stress direction θ as a function of the mean wind direction for the field tests (SoCal2013, SIO pier, and TBL). The wind stress direction is given by

$$\theta = \text{atan2}(-\rho_a \overline{v'w'}, -\rho_a \overline{u'w'}), \quad (6)$$

where atan2 is the four-quadrant arctangent function (defined below), ρ_a is the air density, and $-\rho_a \overline{u'w'}$ and $-\rho_a \overline{v'w'}$ are the stream- and crosswise momentum fluxes expressed in the streamwise wind frame (where the mean wind components V and W are equal to zero). In such a frame, $\theta = 0^\circ$ means that the wind stress is aligned with the wind. The four-quadrant arctangent function is defined in the range $[-\pi; \pi]$ from the standard arctan function by

$$\text{atan2}(x, y) = \begin{cases} \arctan(y/x) & \text{if } x > 0, \\ \arctan(y/x) + \pi & \text{if } x < 0 \text{ and } y \geq 0 \\ \arctan(y/x) - \pi & \text{if } x < 0 \text{ and } y < 0 \\ +\frac{\pi}{2} & \text{if } x = 0 \text{ and } y > 0 \\ -\frac{\pi}{2} & \text{if } x = 0 \text{ and } y < 0 \end{cases}$$

In Figs. 7a,b, each individual 30-min value was reported with a light blue point for CSAT3 measurements and with a light red point for Gill measurements. Bin-averaged data per 15° wind direction bins were reported with a thick blue and a thick red line, respectively, from the CSAT3 and the Gill measurements. We emphasize that in this figure, data points resulted from measurements of an individual anemometer and were independent of the other anemometer. As for the previous figures, the collapse of the data was remarkable for the SoCal2013 dataset. For the SIO pier data, although the spread of the data was large, the shape of the bin-averaged data was comparable to the data from the SoCal2013 and TBL datasets. The three experiments showed that the wind stress direction measured by both anemometers was affected by the wind direction relative to the instruments, as both anemometers measured bin-averaged wind stress direction that deviated from the mean wind direction by up to 20° . The spread of the data for the SIO pier experiment can be explained by two factors. Although the anemometers were mounted on a long boom, placing the instruments as far as possible from the SIO pier, the pier is a bulky structure that created

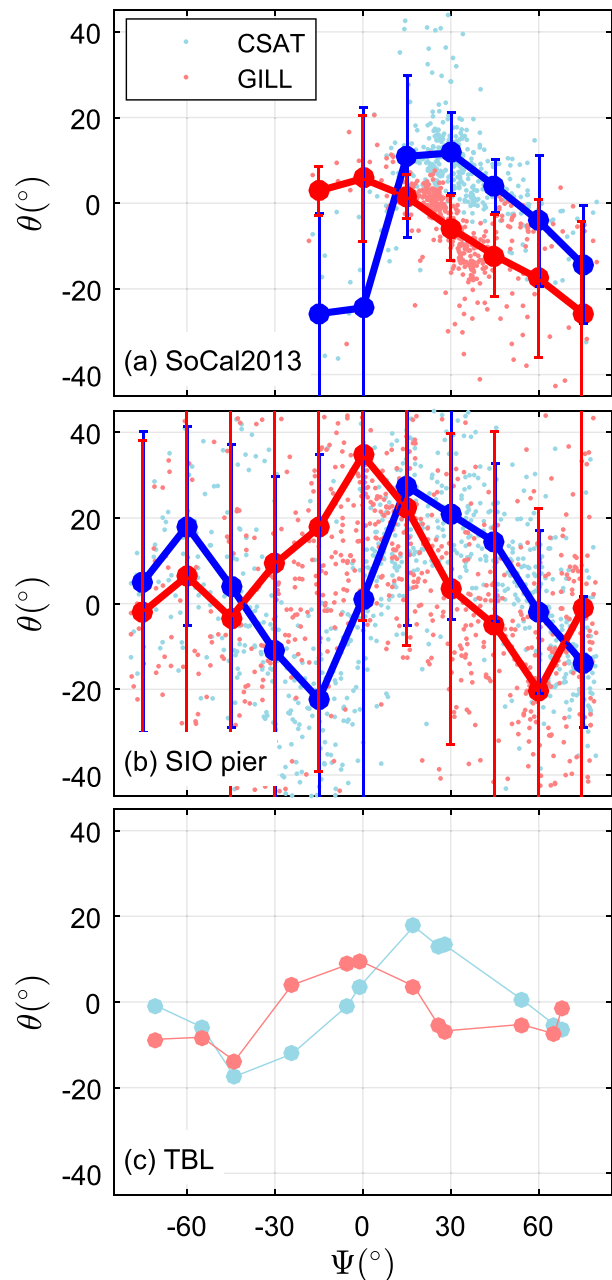


FIG. 7. Stress direction departure θ from the mean wind direction as a function of the wind direction [see Eq. (6) for the definition of θ]. For the SoCal2013 and SIO pier data, 30-min-averaged data points are plotted with light colored points, the bin-averaged values (with their associated error bars) are joined by the thick lines. For the TBL test, the 20-min-averaged values are reported with solid circles joined by a thin line. CSAT3 data are plotted in blue, while Gill data are plotted in red.

flow deflection and additional turbulence. These effects were likely to produce a larger departure of the wind stress direction from the mean wind speed than the SoCal2013 and TBL experiments because, in these last

two experiments, anemometers were farther away from any bulky structure. The second factor was that the wind speed was much smaller during the SIO pier experiment than during the two other field experiments. At smaller winds, the turbulence created by the wind shear is more affected by the presence of waves or by convection than at higher winds. Therefore, at lower winds, it is not surprising that the scatter in the data was larger than at higher winds. Above the ocean surface, it has been shown that the wind stress direction can deviate from the mean wind direction due to the effects of surface waves (Geernaert et al. 1993; Rieder et al. 1994; Grachev et al. 2003), and that the wind stress vector lay between the mean wind and the mean wave directions. From all the data that we gathered above the ocean, a wide range of mean wind and wave directions have been recorded, and we did not find a significant correlation between the wind stress direction and the angle between the mean wind and the mean wave directions. Moreover, since the behaviors of the two anemometers were significantly different, with the CSAT3 data exhibiting an asymmetric pattern around $\Psi = 0^\circ$, while the Gill data exhibited a symmetric pattern, it was difficult to assess which instrument correctly measures the cross component of the wind-stress vector. However, since the departure of the wind-stress direction from the mean wind direction is a phenomenon that depends on several independent environmental variables (convection, large-scale fluctuations of the wind direction, and angle between wind and waves) that are not directly correlated with the wind direction relative to the anemometers, the fact that the wind direction sensitivity of the wind-stress direction departure remained comparable over the three distinct experiments, for both instruments, suggested that this coupling was inherent to the anemometers themselves rather than environmental conditions.

Figure 8 shows the variations of u_* measured by each anemometer as a function of the wind speed and the wind direction. Figures 8a–c show u_* measured by each anemometer as a function of the mean wind speed. For each group of data, the relationship between u_* and U was described by the function $f(U)$, which was the best second-order polynomial fit of the data. Then any measurement of $u_*(\Psi, U)$ was normalized by the azimuthal-averaged value of $\langle u_* \rangle_{\text{azi}} = f(U)$. Therefore, for each anemometer, we computed the relative difference of u_* as

$$\frac{\Delta u_*}{u_*}(\Psi, U) = \frac{u_*(\Psi, U) - f(U)}{f(U)}, \quad (7)$$

which was independent of measurements by the other anemometer. The variation with the wind direction of the bin-averaged ratios of $\Delta u_*/u_*$ measured by the CSAT3 and Gill were plotted in Figs. 8d–f and Figs. 8g–i,

respectively. For the SoCal2013 and pier experiments, data were bin averaged per 15° bins of wind direction for different bins of wind speeds (in color) and for all wind speeds (in black). The correspondence between the color of the lines and the wind speed bins is reported in the color scale in Fig. 8d. Data from the TBL experiment are reported with solid black circles in Figs. 8f,i. We found that for the three experiments, the values of u_* measured by the Gill were quite insensitive to the wind direction and remained, on average, constant within a $\pm 10\%$ range. However, data from the CSAT3 showed that the estimate of u_* depended on the wind direction for all wind speeds. The relative difference varied by $\pm 20\%$, which meant that for the same wind speed, depending on the wind direction, the difference between estimates of u_* can be as large as 40%.

Figure 9 shows the normalized cumulative cospectra between u' and w' bin averaged for different wind directions. The left panels correspond to data measured by the CSAT3 and the right panels correspond to data from the Gill, measured during the SoCal2013, SIO pier, and TBL tests. The value of the cumulative cospectrum at the frequency f was equal to the integration of the cospectrum function between u' and w' from the highest frequency (i.e., $f_h = 10$ Hz) down to f . As previously done for the data presented in Fig. 8, the cumulative cospectra of each anemometer were normalized by the square of their azimuthal-averaged friction velocity, $\langle u_* \rangle_{\text{azi}} = f(U)$, and then bin averaged by wind direction. The color bar at the top of the figure indicates the range of wind directions for each bin-averaged curve reported in Fig. 9. As in Fig. 8, Fig. 9 shows that the cospectra of $u'w'$ computed from CSAT3 measurements were strongly affected by the wind direction, while the dependence was rather weak for the measurements from the Gill anemometer. When the wind was aligned with the CSAT3 (gray curves in Figs. 9a,c,e), the cumulative cospectra exhibited abnormally weak values in the high-frequency range. For all experiments, the cumulative cospectrum was null or even positive for frequencies greater than 0.2–0.4 Hz, which meant that frequencies greater than 0.2–0.4 Hz did not support any downward momentum flux. On the contrary, positive values of the cumulative cospectrum at high frequencies suggested that these frequencies would be responsible for an upward momentum flux—that is, from the surface (waves or ground) toward the airflow—that was unlikely to happen in a turbulent boundary layer in the high-frequency range.² This effect produced final values (at the

² In the presence of fast waves (swell) or when the boundary layer was strongly unstable under the effect of large convective cells, upward momentum flux has been measured both over ground and waves and was supported by lower frequencies, say, less than $O(0.1)$ Hz.

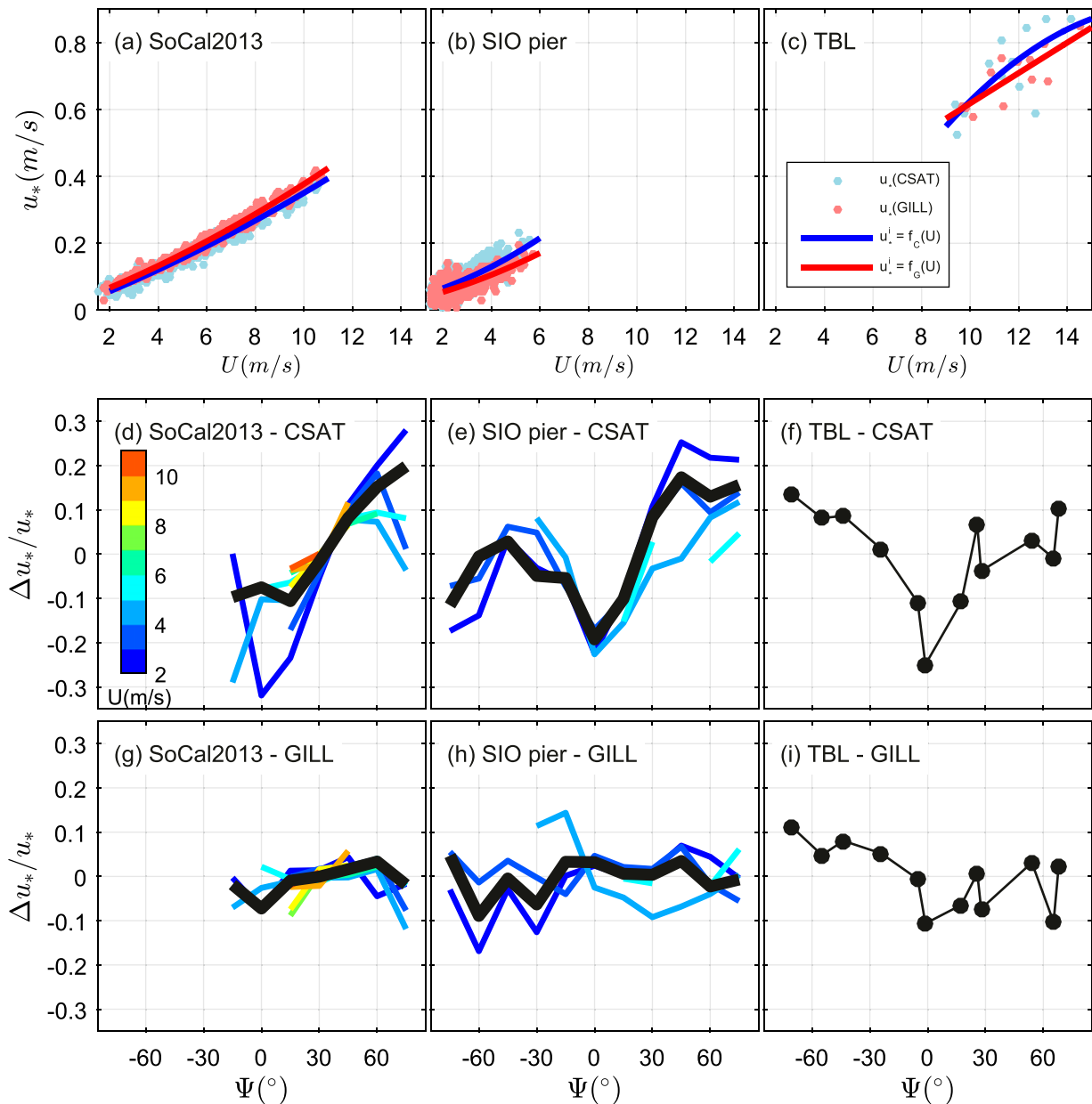


FIG. 8. (left) SoCal2013 experiment, (middle) SIO pier experiment, and (right) TBL experiment. (a)–(c) the friction velocity u_* measured by the CSAT3 (blue) and the Gill (red) as a function of the mean wind speed. The light colored dots are 30-min (20 min for the TBL experiment) data points. The thick lines correspond to the best fits for $u_* = f(U)$, where f is a second-order polynomial function. (d)–(f) The relative difference in the friction velocity $\Delta u_*/u_* = [u_*(\Psi, U) - \langle u_* \rangle_{azi}] / \langle u_* \rangle_{azi}$ as a function of the wind direction for the CSAT3 data. The azimuthal-averaged friction velocities $\langle u_* \rangle_{azi}$ are calculated according to the best functions $u_* = f(U)$ from the respective upper panels. Colored lines show the variations of the relative difference per wind speed bins for different wind speeds corresponding to the color scale in (d). The thick black line represents the variation of the relative difference averaged over all wind speeds. (g)–(i) As in (d)–(f), but for the Gill data.

lowest resolved frequency $f = f_i$) of the cumulative cospectrum that were too low compared to the reference value, leading to an underestimation of the momentum flux of up to 40%. When the wind was coming from the side, the shape of the cumulative cospectra was classical

(i.e., high frequencies supporting downward momentum flux); nevertheless, the final values of the normalized cumulative cospectra fell in the range $[-1.4, -1]$, meaning that the momentum flux was overestimated by up to 40%. On the other hand, cumulative cospectra from the Gill

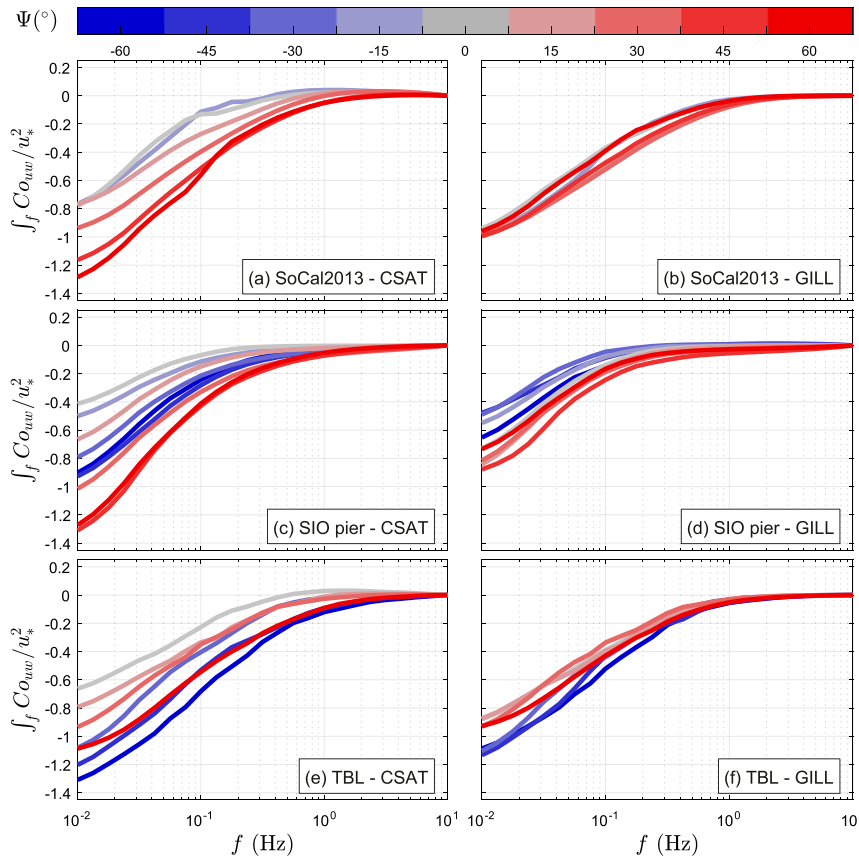


FIG. 9. Cumulative cospectra of $u'w'$ for different bins of wind direction for the (left) CSAT3 and (right) Gill measurements. The cumulative cospectra are scaled by the azimuthal-averaged friction velocity $\langle u_* \rangle_{azi} = f(U)$ obtained from the best functions presented in Figs. 8a–c. (from top to bottom) SoCal2013, SIO pier, and TBL experiments. Lines are color coded by wind direction bins according to the color bar at the top of the figure.

exhibited the same shape and final values close to one. The spread in the data observed for the SIO pier data was likely due to the crosswind cospectrum $\overline{v'w'}$ whose effects became stronger in these low wind conditions. Large spreading of the data was already observed in Fig. 7b.

4. Discussion

We found that the discrepancies observed between the CSAT3 and Gill measurements were mainly driven by the wind direction relative to the instruments. The relative difference in the mean wind speed between anemometers was a few percent, which corresponds to the manufacturers' stated ranges of accuracy. Data from the wind tunnel in a quasi-laminar flow suggested that the Gill measurements were insensitive to the wind direction, as the mean wind speed and the mean wind direction were in agreement with reference values (Pitot measurements and physical rotation of the instruments)

with less than 1% error for the mean wind speed and less than 1° deviation for the wind direction. However, for the CSAT3, the relative difference in the mean wind speed varies from -2% to +1% and the absolute difference in the mean wind direction varied from -2° to +2° depending on the wind direction. Applying the transducer shadowing correction (TSC) on the CSAT3 data increased on average the mean wind speed compared to those measured by the Gill. On the other hand, it did not reduce the wind direction variability between the instruments for both the mean wind speed and direction.

In the field, the intercomparison between the two anemometers revealed that the dependence on the wind direction of the difference in both the mean wind speed and the mean wind direction was comparable to that observed in the wind tunnel. This suggested that the Gill maintained its accuracy, at least for the mean wind speed and the mean wind direction, in a turbulent flow, and that the measurement differences from the CSAT3 likely persisted

in a turbulent flow. Regarding the Gill, the applicability of a calibration performed in a laminar flow to a turbulent flow has been discussed previously in Hogstrom and Smedman (2004). They suggested that the wakes generated by the three rods of the Gill cage differed from laminar flow to turbulent flow, implying that the calibration cannot be reliably transferred to measurements in a turbulent flow. The effect of those wakes on the measurements was likely to be important when the rods are upwind of the measuring volume (which corresponds in our case to $\Psi = \pm 60^\circ$). Although we share the point of view of Hogstrom and Smedman (2004), our data did not present significant evidence that the measurements of the mean wind speed and direction from the Gill were affected when Ψ was in the neighborhood of $\pm 60^\circ$. Nevertheless, a detailed analysis of the influence of the rods in a turbulent flow is required to clarify this point.

Is flow interference created by the body of the CSAT3? This hypothesis is supported by the asymmetric difference in the mean wind direction, especially in the wind tunnel. Indeed, in the wind tunnel, when the CSAT3 was oriented at $+60^\circ$ from the axis of the wind tunnel, it measured a wind direction relative to the instrument equal to approximately 62° . The opposite happened when $\Psi = -60^\circ$ (the instrument measured -62°). If we assumed that the wind direction was correctly measured by the CSAT3, it would mean that the streamlines were deflected from the body of the anemometer. But as the differences with the Gill showed a pattern in the field consistent with the observations in the wind tunnel, and assuming that the Gill is correctly calibrated for its own flow distortion, it is reasonable to think that the flow distortion around the body of the CSAT3 persisted in the field experiment.

Regarding the CSAT3, there have been relatively very few comparisons against a reference instrument (Grelle and Lindroth 1994; Horst et al. 2015). On the contrary, the CSAT3 has been intensively used as the instrument of reference during intercomparison studies (Loescher et al. 2005; Mauder et al. 2007; Nakai et al. 2014).

Measurements of the standard deviation of the vertical wind components have shown that the difference between instruments was also sensitive to the wind direction. Averaged over all the wind directions studied, the difference between instruments was quite small (less than 2%). However, when the TSC was applied, the wind direction variability remained,³ but on average, the CSAT3 values of σ_w were about 5% larger than those

from the Gill. As has been recently discussed by Horst et al. (2015) and Frank et al. (2016), using the Kaimal correction for the transducer shadowing was helpful to reduce the gap between orthogonal and nonorthogonal (CSAT3) anemometers in their estimation of the magnitude of w' . Our results suggest that the magnitude of w may be underestimated by the Gill. Using the Kaimal correction, Horst et al. (2015) and Frank et al. (2016) have shown that underestimation of the magnitude of w' was more sensitive to the angle of attack than to the wind direction. But for our experiments, the angle of attack was mainly in a small range, between -15° and $+15^\circ$ (see Fig. 10); it was therefore difficult to assess the role of the angle of attack on the difference between the two anemometers in the estimation of w' .

We also have shown that the friction velocity measured by the two anemometers can differ by 20% in moderate to strong winds, while it differed by up to 40% at lower winds. Although discrepancies between the different experiments prevent us from drawing definitive quantitative conclusions, all experiments showed that the relative difference in u_* between instruments reached a minimum when the wind was aligned with the anemometers. The data corrected for the transducer shadowing showed that the correction was effective in reducing the wind direction variability of the wind stress discrepancy between instruments.

In conjunction with this effect, we have shown that for both instruments the departure of the wind stress direction from the mean wind direction was up to 20° – 30° when data were bin averaged. The instruments showed distinct behaviors, the CSAT3 having an asymmetric response as a function of the wind direction [i.e., zero departure at $\Psi = 0^\circ$, positive (negative) departure when Ψ was positive (negative), with maximum departure around $\Psi = \pm 30^\circ$]. The Gill had a symmetric response with the maximum departure reached at $\Psi = 0^\circ$. The consistency of these patterns among the three field experiments suggested that this wind stress departure may be inherent to the instruments rather than environmental variables. Once again, applying the transducer shadowing correction to the CSAT3 data decreased the amplitude of the variations with the wind direction of the departure of the wind stress direction from the wind direction.

An intercomparison between instruments can only point out differences between the two. Reference measurements are of crucial importance to determine the accuracy of an instrument. But conducting reference measurements is not an easy task, even in a wind tunnel. It requires the reference instrument to be fully calibrated both in laminar and turbulent flows, and for it to remain insensitive to variations of the wind direction

³ The direct comparison between the uncorrected (raw) and the corrected (TSC) data from the CSAT3 showed that the correction slightly reduced the wind direction variability by less than 1%, which explained why we barely see the reduction in Fig. A3.

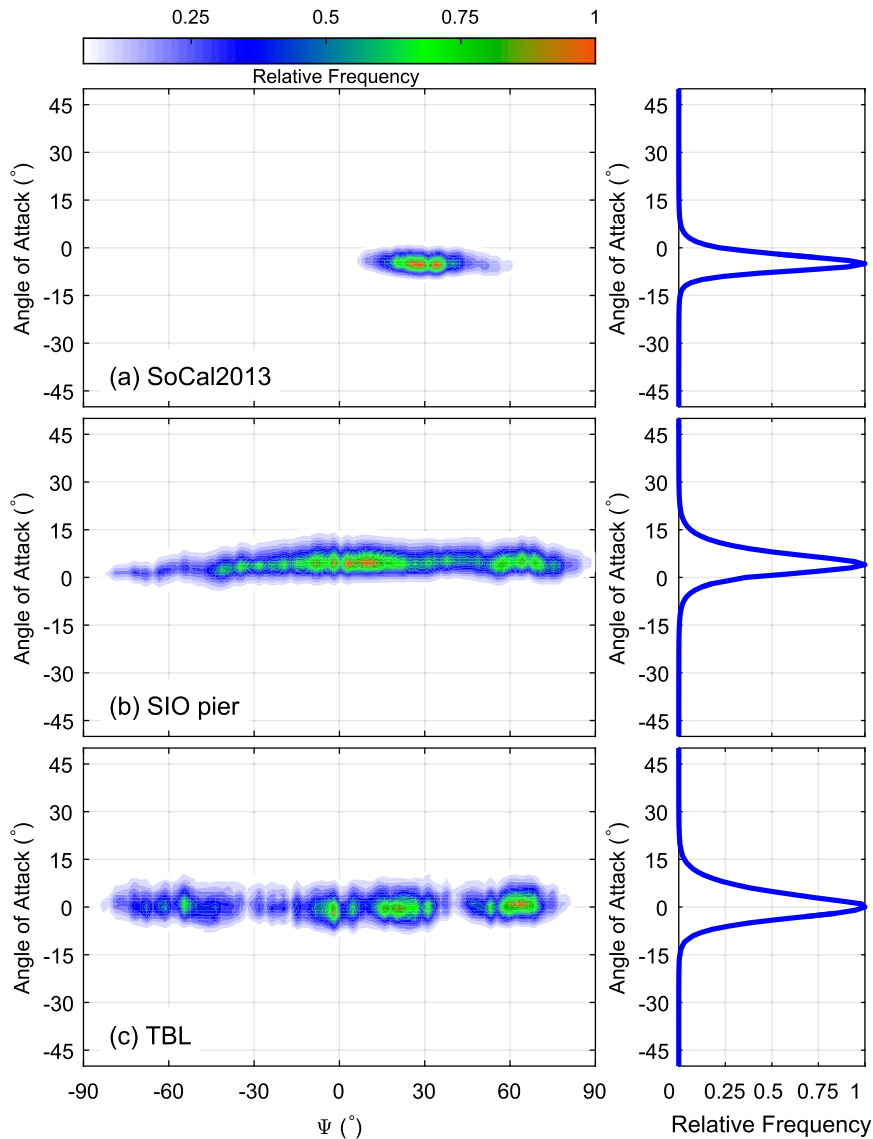


FIG. 10. Normalized histogram of horizontal wind direction and vertical angle of attack from all 20-Hz sonic anemometer measurements used to construct the datasets for the (a) SoCal2013, (b) SIO pier, and (c) TBL experiments. Each histogram is normalized by its maximum value.

and the angle of attack while collocated with the volume of measurement of the tested anemometer.

During our field experiments, no reference instrument was available. Hence, in order to analyze independently the wind direction sensitivity of each instrument, we computed azimuthal-averaged friction velocity, which depended only on the wind speed regardless of the wind direction, and we analyzed the variations with the mean wind direction of the difference between the measured friction velocities and these averaged values. This method was very effective in highlighting the wind direction sensitivity of the CSAT3 in its estimates of u_* and the

covariance $\overline{u'w'}$. The measured values of u_* were found to be 20% smaller than the azimuthal averages when the CSAT3 was aligned with the wind, increasing up to 10%–20% higher than the azimuthal averages when the wind direction was larger than 30°. This trend was observed for all field datasets. This wind direction sensitivity was not observed for the Gill.

The wind direction dependency has been further analyzed looking at the cumulative cospectra between u' and w' . When normalized by the square of the reference value of u_* , the results showed that the CSAT3 can underestimate the momentum flux by up to 50% (50%

TABLE 1. Manufacturers' specifications for CSAT3 and Gill.

	Range of application	Wind speed range (m s^{-1})	Wind speed accuracy	Wind speed resolution	Zero offset (m s^{-1})	Wind direction accuracy	Wind direction resolution
CSAT3	Wind incidence within $\pm 5^\circ$ of horizontal		$\pm 2\%$ of reading				
	Wind incidence within $\pm 10^\circ$ of horizontal	< 30	$\pm 3\%$ of reading	$u_x, u_y \leq 1 \text{ mm s}^{-1}$	$u_x, u_y < \pm 0.08$	$\pm 0.7^\circ$ at 1 m s^{-1}	
	Wind incidence within $\pm 20^\circ$ of horizontal		$\pm 6\%$ of reading	$u_z \leq 0.5 \text{ mm s}^{-1}$	$u_z < \pm 0.04$		
Gill	Wind incidence within $\pm 20^\circ$ of horizontal	< 50	$< 1\%$ RMS	0.01 m s^{-1}	≤ 0.01		$\leq \pm 1^\circ$

at low winds, 25%–35% for moderate and high winds) when the instrument was aligned with the wind. This underestimation came from coherent fluctuations between u' and w' at high frequencies that generated an artificial upward momentum flux that counterbalanced the expected downward momentum flux characteristic of turbulent boundary layers. On the other hand, when the wind came from the right or the left of the CSAT3, although there were discrepancies between datasets, the CSAT3 overestimated the momentum flux between 10% and 30% when the wind direction was greater than 30° – 45° . The cumulative cospectra between u' and w' measured by the Gill exhibited shapes that remained very similar for any wind direction and for all datasets.

The introduction of the azimuthal averages of u_* clearly highlighted the sensitivity of CSAT3 measurements to the wind direction while showing a good response of the Gill in the same conditions. This result was consistent with the relative difference in the mean wind speed and direction observed in the wind tunnel. It also suggested that the discrepancies we observed between the two instruments were likely due to errors in the CSAT3 measurements.

5. Conclusions

For the last decade, the CSAT3 sonic anemometer has been extensively used as the reference instrument for field campaigns and for intercomparison studies (Loescher et al. 2005; Mauder et al. 2007; Nakai and Shimoyama 2012). Although our data showed that the CSAT3 measurement differences were within the manufacturer's specifications for the mean wind speed and wind direction (see Table 1), its accuracy in measuring momentum flux still remained uncertain.

Our study has revealed that measurements from CSAT3 and Gill sonic anemometers significantly differ and that these differences are strongly correlated with the wind direction relative to the instruments. Comparisons

between reference (Pitot tube) and azimuthal-averaged values reveal that the measurements from the CSAT3 are affected by the wind direction, while the Gill shows a weak sensitivity to the wind direction, which suggests that the differences observed between the two anemometers can be for the most part attributed to CSAT3 measurement errors. The Kaimal correction of the transducer shadowing (following Horst et al. 2015) has shown potential in reducing the gap between the two anemometers, although it did not entirely remove the wind direction sensitivity of the discrepancies between the two anemometers. Since both sonic anemometers have been extensively used over the past decade to measure fluxes (momentum, heat, moisture) both over land and sea, a comprehensive study to quantify their accuracy in measuring the mean wind vector and the stress vector needs to be conducted against a reference instrument, both in a controlled environment and in the field. In the past, intercomparisons between instruments and wind tunnel calibrations have shown some limitations in assessing the accuracy of sonic anemometers. We think that the development of new techniques are required to correctly estimate the accuracy of commercially available sonic anemometers. We think that using laser Doppler velocimetry (LDV) or particle image velocimetry (PIV) in wind tunnels (if possible under turbulent flow generated by turbulence grids) would help characterize possible flow distortion around anemometers. Also, the development of wind lidar measurements make possible the characterization of the accuracy of sonic anemometers in the field. Recent work from Dellwik et al. (2014) brought exciting perspectives in that regard.

Acknowledgments. We thank Tom Golfinos, Capt. Bill Gaines, and the crew of the R/P *FLIP* for their support during the SoCal2013 experiment. The measurements would not have been possible without the work of Nick Statom, Peter Sutherland, Luc Deike, and Daniel Moskowitz. We also thank Gregory Morris for

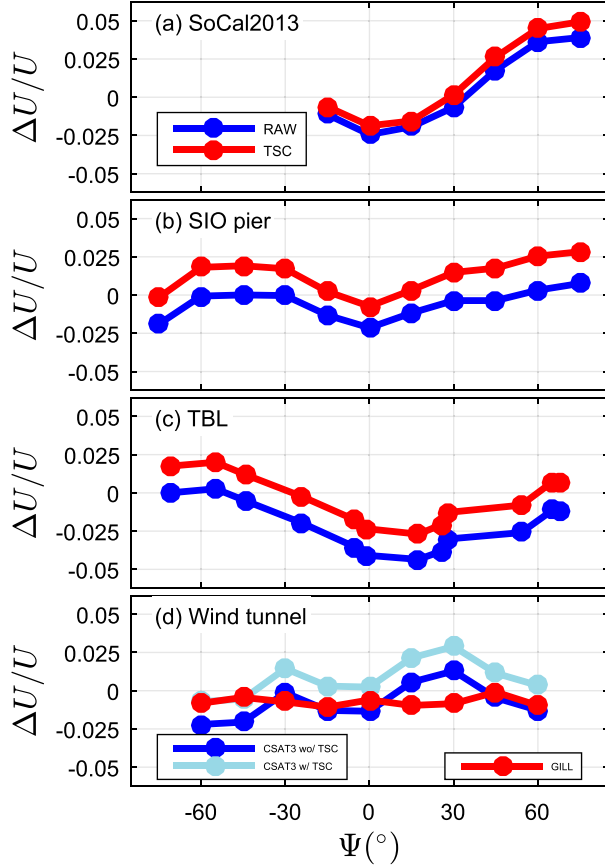


FIG. A1. Relative difference in the mean wind speed $\Delta U/U$ as a function of the mean wind direction. See Eq. (3) for the definition of $\Delta U/U$. For the SoCal2013 and SIO pier experiments, only bin-averaged data are plotted. (a)–(c) The raw data (blue) correspond to CSAT3 measurements not corrected for the transducer shadowing, while the TSC data (red) correspond to CSAT3 measurements where TSC was applied. (d) Raw CSAT3 data are plotted in dark blue, CSAT3 data with the TSC are in light blue, and Gill data are in red.

his support during the collection of data in the SDSU wind tunnel. We thank three anonymous referees for their comments and questions, which led to significant improvements in the paper. This research was supported by grants to WKM from ONR (Code32; N00014-12-1-1022 and N00014-14-1-0710) and NSF (OCE 1155403).

APPENDIX

CSAT3 Measurements Corrected for the Transducer's Shadowing Attenuation

The recent publications from of Horst et al. (2015) and Frank et al. (2016) have shown that the CSAT3 suffers from the fact that it is not corrected for transducer shadowing. Both authors have shown that applying the Kaimal correction (Kaimal 1978) to the CSAT3 data was

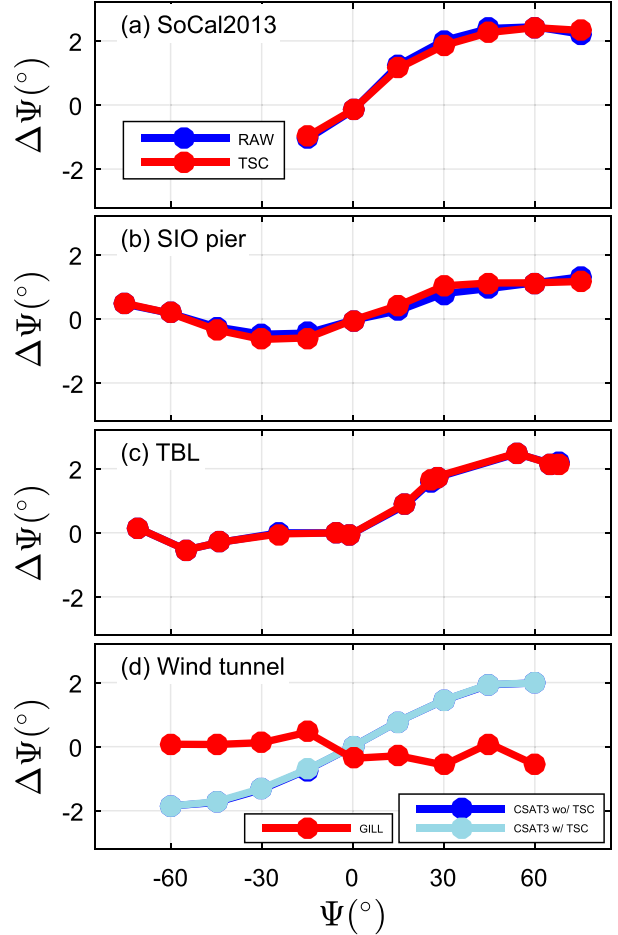


FIG. A2. As in Fig. A1, but for the difference in the mean wind direction $\Delta\Psi$.

useful in explaining some discrepancies observed between CSAT3 and orthogonal sonic anemometers. Therefore, we applied this correction to our CSAT3 datasets and compared the solutions to both the CSAT3 and Gill raw datasets. The datasets were corrected following the method used by Horst et al. (2015) for each 20-Hz sample:

- 1) The measured raw velocity components $\{\hat{u}, \hat{v}, \hat{w}\}$ were transformed into the transducer's path components $\{\hat{u}_a, \hat{u}_b, \hat{u}_c\}$.
- 2) The angle θ_i of each path relative to the wind was calculated as

$$\theta_i = \cos^{-1}(\hat{u}_i/\sqrt{\hat{u}^2 + \hat{v}^2 + \hat{w}^2}), \quad i = a, b, c. \quad (\text{A1})$$

- 3) Each path component is corrected for the transducer shadowing,

$$u_i = \hat{u}_i/(0.84 + 0.16 \sin\theta_i), \quad i = a, b, c, \quad (\text{A2})$$

where u_i are the corrected components.

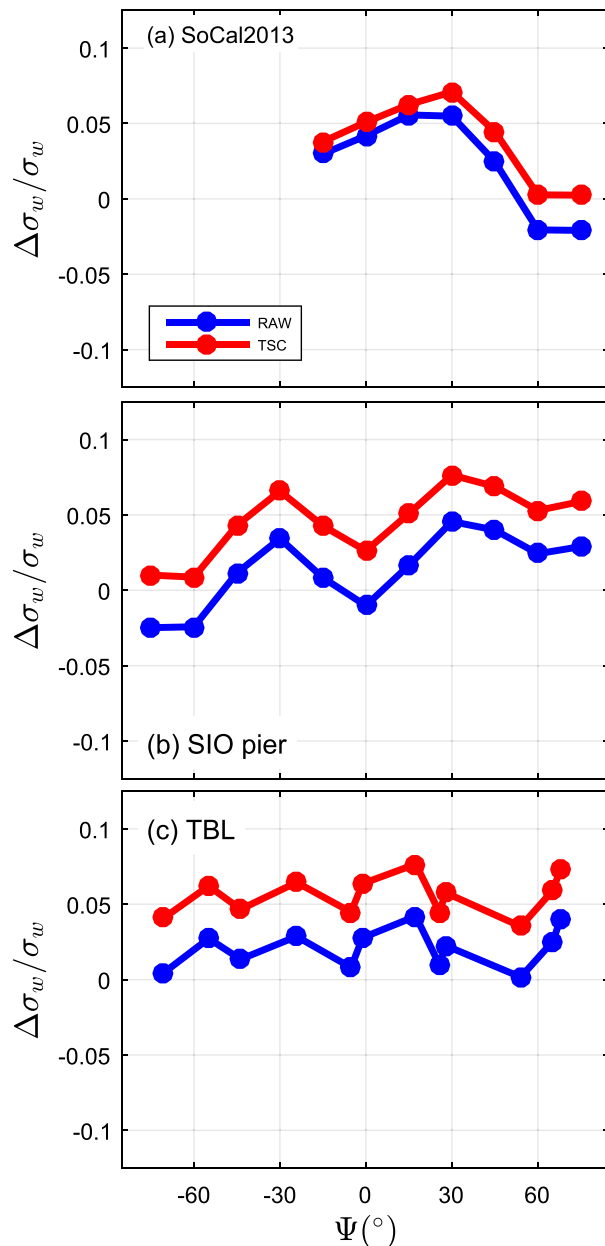


FIG. A3. As in Fig. A1, but for σ_w (the relative difference in the standard deviation of w) and only for the SoCal2013, SIO pier, and TBL experiments.

- 4) The corrected path components $\{u_a, u_b, u_c\}$ are transformed back into the orthogonal instrument frame $\{u, v, w\}$.

This sequence was iterated three times, so at the beginning of the second (third) iteration, components $\{\hat{u}, \hat{v}, \hat{w}\}$ are replaced by the solution of the first (second) iteration $\{u, v, w\}$. This iterative scheme ensured that the path wind angles θ_i and the wind speed amplitude $\sqrt{\hat{u}^2 + \hat{v}^2 + \hat{w}^2}$ are computed using values corrected for the transducer shadowing.

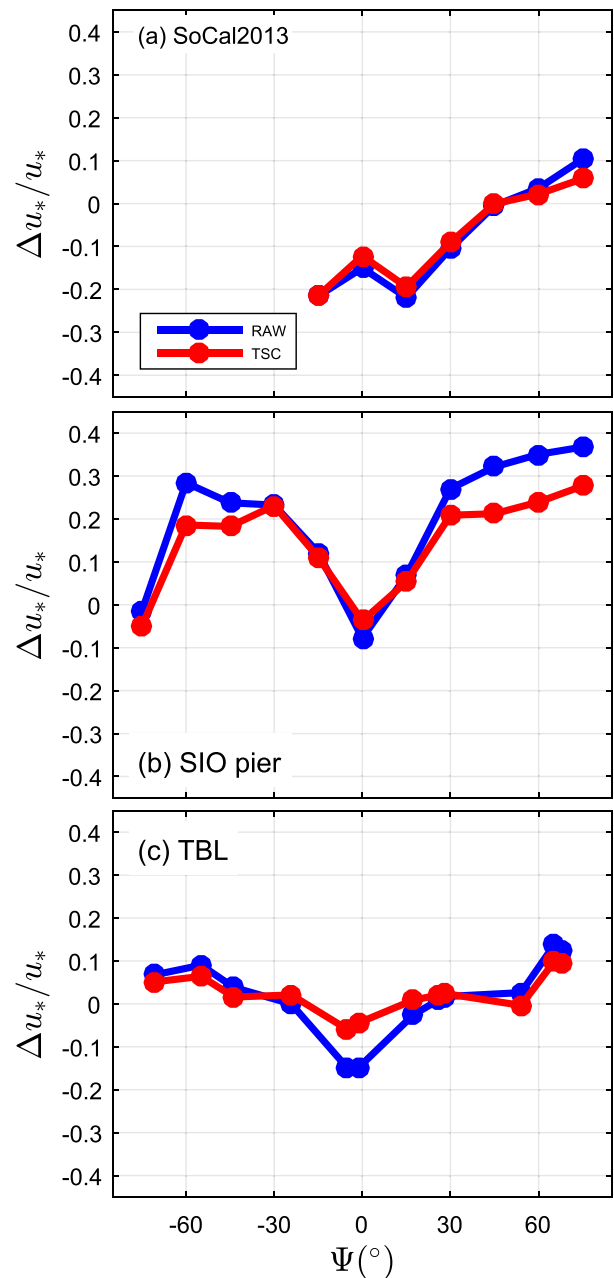


FIG. A4. As in Fig. A3, but for the relative difference in the friction velocity u_* .

Relative differences in the mean wind speed as a function of the mean wind direction are presented in Fig. A1. Hereinafter, for the SoCal2013 and SIO pier experiments, only bin-averaged data are plotted. For the field experiments, the relative differences between the uncorrected (labeled “raw”) CSAT3 data and the Gill were plotted in blue and the relative difference between the corrected [labeled transducer shadowing correction (TSC)] were plotted in red. As in the main part of the manuscript, the differences between

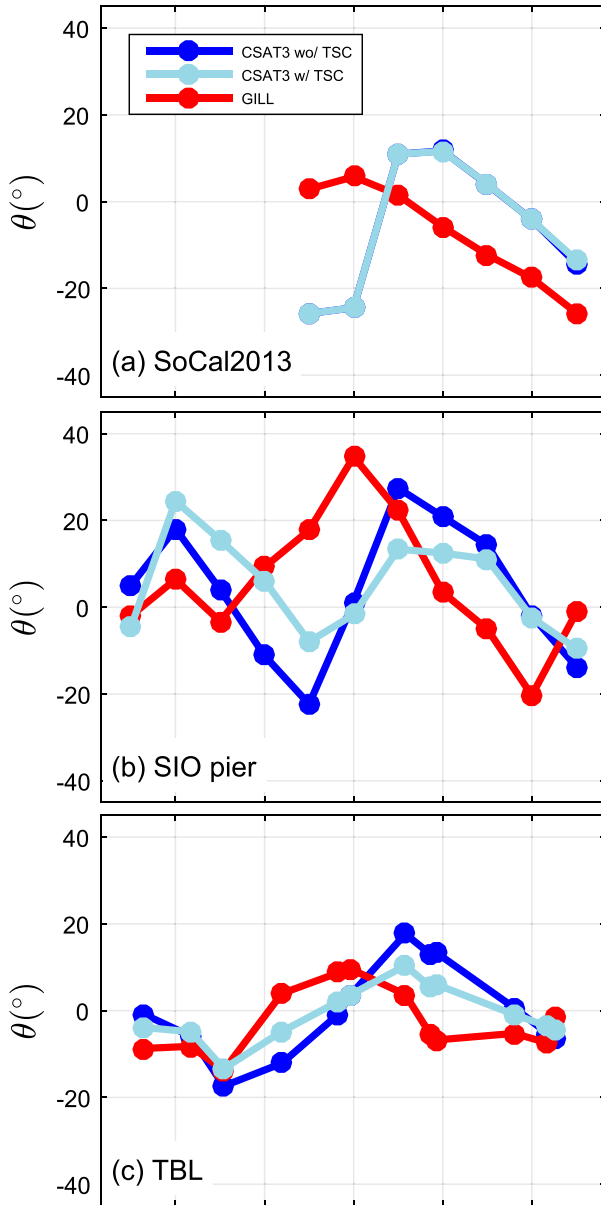


FIG. A5. Stress direction departure θ from the wind direction as function of the wind mean direction. Dark blue solid circles correspond to raw CSAT3 data, light blue circles correspond to CSAT3 measurements corrected for the transducer shadowing effects, and red circles correspond to Gill data.

instruments were scaled by the averaged values of the considered variables, with and without the correction, that is, $(\Delta U/U)_{\text{RAW}} = 2(U_{\text{RAW}} - U_{\text{Gill}})/(U_{\text{RAW}} + U_{\text{Gill}})$ and $(\Delta U/U)_{\text{TSC}} = 2(U_{\text{TSC}} - U_{\text{Gill}})/(U_{\text{TSC}} + U_{\text{Gill}})$.

For the wind tunnel experiment, the relative difference between the raw (TSC) CSAT3 data and the reference Pitot tube were plotted in dark (light) blue; the difference between the Gill and the Pitot tube was plotted in red. When the correction was applied, it increased the mean wind

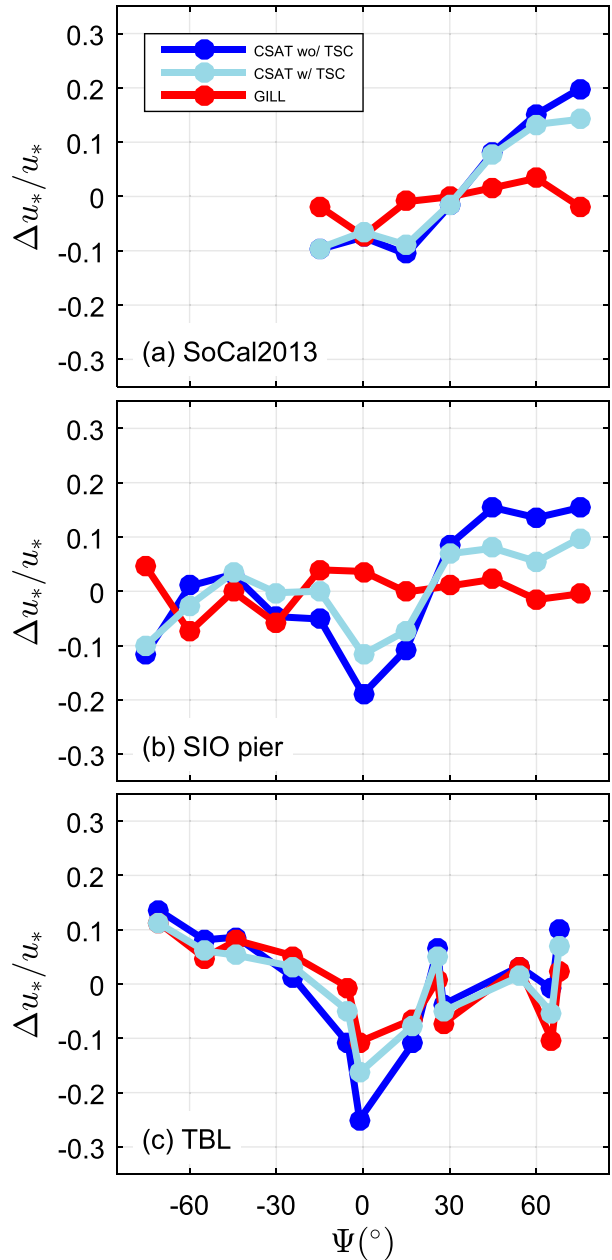


FIG. A6. Relative difference in the friction velocity between measured u_{*X} and computed azimuthal-averaged friction velocity $\langle u_* \rangle_{\text{azi}}$ as a function of the mean wind direction as in Figs. 8d–i, $\Delta u_*/u_* = (u_{*X} - \langle u_* \rangle_{\text{azi}})/\langle u_* \rangle_{\text{azi}}$, where the subscript X corresponds to the anemometer dataset plotted. Dark blue solid circles correspond to raw CSAT3 data, light blue circles correspond to CSAT3 measurements corrected for the transducer shadowing, and red circles correspond to Gill data.

speed by about 2%, but it barely affected the variations with the wind direction. This last point was consistent with the results from Horst et al. (2015, their Fig. 7, upper panel).

The differences in the mean wind direction as a function of the mean wind direction are presented in Fig. A2.

It shows that applying the correction did not change the wind direction measured by the CSAT3 in the field nor in the wind tunnel.

The differences in the standard deviation of the vertical component of the wind as a function of the mean wind direction are presented in Fig. A3. As for the mean wind speed, the correction led to an increase of the standard deviation by about 3%–4%, but it did not affect the wind direction sensitivity of the difference between the CSAT3 and the Gill. This is also consistent with the simulated attenuation by transducer shadowing performed by Horst et al. (2015, their Fig. 6, top panel). Ignoring the SoCal2013 experiment (because of the anemometer height difference), the relative differences averaged over all wind directions were about 1%–2% without the correction and about 5% with the correction, the CSAT3 measuring higher values than the Gill.

The differences between anemometers in the friction velocity as a function of the mean wind direction are presented in Fig. A4. For this variable, the correction did not affect much the wind direction–averaged relative difference, but it reduced the variability associated with the wind direction.

The departures θ of the stress direction from the wind direction for each anemometer as a function of the wind direction are presented in Fig. A5. As for the friction velocity, the correction improved the solution, as the wind direction variability became smaller when the correction was applied.

Finally, the relative differences in u_* from the azimuthal averages of u_* as a function of the mean wind direction were plotted in Fig. A6. Once again, applying the correction reduced the wind direction variability, even though this variability remained larger for the CSAT3 than what was observed for the Gill.

In conclusion, the Kaimal correction for the transducer shadowing reduced the wind direction dependency of the differences observed between the CSAT3 and the Gill.

REFERENCES

- Campbell Scientific, Inc., 2015: CSAT3 three dimensional sonic anemometer instruction manual. Revision 2/15, 74 pp. [Available online at <https://s.campbellsci.com/documents/us/manuals/cs3.pdf>.]
- Dellwik, E., J. Mann, M. Sjöholm, N. Angelou, and T. Mikkelsen, 2014: Comparison of three-dimensional wind measurements by wind-lidars and a sonic anemometer. *Extended Abstracts, 14th EMS Annual Meeting/10th European Conf. on Applied Climatology (ECAC)*, Prague, Czech Republic, European Meteorological Society, EMS2014-277. [Available online at <http://meetingorganizer.copernicus.org/EMS2014/EMS2014-277.pdf>.]
- Edson, J. B., A. A. Hinton, K. E. Prada, J. E. Hare, and C. W. Fairall, 1998: Direct covariance flux estimates from mobile platforms at sea. *J. Atmos. Oceanic Technol.*, **15**, 547–562, doi:10.1175/1520-0426(1998)015<0547:DCFEM>2.0.CO;2.
- Frank, J. M., W. J. Massman, and B. E. Ewers, 2013: Underestimates of sensible heat flux due to vertical velocity measurement errors in non-orthogonal sonic anemometers. *Agric. For. Meteorol.*, **171–172**, 72–81, doi:10.1016/j.agrformet.2012.11.005.
- , —, E. Swiatek, H. A. Zimmerman, and B. E. Ewers, 2016: All sonic anemometers need to correct for transducer and structural shadowing in their velocity measurements. *J. Atmos. Oceanic Technol.*, **33**, 149–167, doi:10.1175/JTECH-D-15-0171.1.
- Geernaert, G. L., F. Hansen, M. Courtney, and T. Herbers, 1993: Directional attributes of the ocean surface wind stress vector. *J. Geophys. Res.*, **98**, 16 571–16 582, doi:10.1029/93JC01439.
- Gill Instruments Ltd., 2005: Omnidirectional (R3-50) ultrasonic anemometer user manual. Doc. 1210-PS-0011, Issue 04, 67 pp. [Available online at gillinstruments.com/data/manuals/r3-50-manual.pdf?iss=4.20150501.]
- Grachev, A. A., C. W. Fairall, J. E. Hare, J. B. Edson, and S. D. Miller, 2003: Wind stress vector over ocean waves. *J. Phys. Oceanogr.*, **33**, 2408–2429, doi:10.1175/1520-0485(2003)033<2408:WSVOOW>2.0.CO;2.
- Grelle, A., and A. Lindroth, 1994: Flow distortion by a Solent sonic anemometer: Wind tunnel calibration and its assessment for flux measurements over forest and field. *J. Atmos. Oceanic Technol.*, **11**, 1529–1542, doi:10.1175/1520-0426(1994)011<1529:FDBASS>2.0.CO;2.
- Hogstrom, U., and A.-S. Smedman, 2004: Accuracy of sonic anemometers: Laminar wind-tunnel calibrations compared to atmospheric in situ calibrations against a reference instrument. *Bound.-Layer Meteorol.*, **111**, 33–54, doi:10.1023/B:BOUN.0000011000.05248.47.
- Horst, T. W., S. R. Semmer, and G. Maclean, 2015: Correction of a non-orthogonal, three-component sonic anemometer for flow distortion by transducer shadowing. *Bound.-Layer Meteorol.*, **155**, 371–395, doi:10.1007/s10546-015-0010-3.
- Kaimal, J., 1978: Sonic anemometer measurement of atmospheric turbulence. *Proceedings of the Dynamic Flow Conference 1978 on Dynamic Measurements in Unsteady Flows*, B. W. Hansen, Ed., Springer, 551–565, doi:10.1007/978-94-009-9565-9_29.
- Kochendorfer, J., T. Meyers, J. Frank, W. Massman, and M. Heuer, 2012: How well can we measure the vertical wind speed? Implications for fluxes of energy and mass. *Bound.-Layer Meteorol.*, **145**, 383–398, doi:10.1007/s10546-012-9738-1.
- Loescher, H., and Coauthors, 2005: Comparison of temperature and wind statistics in contrasting environments among different sonic anemometer–thermometers. *Agric. For. Meteorol.*, **133**, 119–139, doi:10.1016/j.agrformet.2005.08.009.
- Mauder, M., 2013: A comment on “How well can we measure the vertical wind speed? Implications for fluxes of energy and mass” by Kochendorfer et al. *Bound.-Layer Meteorol.*, **147**, 329–335, doi:10.1007/s10546-012-9794-6.
- , and Coauthors, 2007: The energy balance experiment EBEX-2000. Part II: Intercomparison of eddy-covariance sensors and post-field data processing methods. *Bound.-Layer Meteorol.*, **123**, 29–54, doi:10.1007/s10546-006-9139-4.
- Meyers, T., and M. Heuer, 2006: A field methodology to evaluate sonic anemometer angle of attack errors. 27th Conf. on Agricultural and Forest Meteorology, San Diego, CA, Amer. Meteor. Soc., 1.8A. [Available online at <https://ams.confex.com/ams/BLTAgFBioA/webprogram/Paper114559.html>.]
- Nakai, T., and K. Shimoyama, 2012: Ultrasonic anemometer angle of attack errors under turbulent conditions. *Agric. For. Meteorol.*, **162–163**, 14–26, doi:10.1016/j.agrformet.2012.04.004.

- , M. van der Molen, J. Gash, and Y. Kodama, 2006: Correction of sonic anemometer angle of attack errors. *Agric. For. Meteor.*, **136**, 19–30, doi:[10.1016/j.agrformet.2006.01.006](https://doi.org/10.1016/j.agrformet.2006.01.006).
- , H. Iwata, Y. Harazono, and M. Ueyama, 2014: An inter-comparison between Gill and Campbell sonic anemometers. *Agric. For. Meteor.*, **195–196**, 123–131, doi:[10.1016/j.agrformet.2014.05.005](https://doi.org/10.1016/j.agrformet.2014.05.005).
- Rieder, K. F., J. A. Smith, and R. A. Weller, 1994: Observed directional characteristics of the wind, wind stress, and surface waves on the open ocean. *J. Geophys. Res.*, **99**, 22 589–22 596, doi:[10.1029/94JC02215](https://doi.org/10.1029/94JC02215).
- van der Molen, M., J. Gash, and J. Elbers, 2004: Sonic anemometer (co)sine response and flux measurement: II. The effect of introducing an angle of attack dependent calibration. *Agric. For. Meteor.*, **122**, 95–109, doi:[10.1016/j.agrformet.2003.09.003](https://doi.org/10.1016/j.agrformet.2003.09.003).
- Vickers, D., and L. Mahrt, 1997: Quality control and flux sampling problems for tower and aircraft data. *J. Atmos. Oceanic Technol.*, **14**, 512–526, doi:[10.1175/1520-0426\(1997\)014<0512:QCAFSP>2.0.CO;2](https://doi.org/10.1175/1520-0426(1997)014<0512:QCAFSP>2.0.CO;2).
- Wilczak, J., S. Oncley, and S. Stage, 2001: Sonic anemometer tilt correction algorithms. *Bound.-Layer Meteor.*, **99**, 127–150, doi:[10.1023/A:1018966204465](https://doi.org/10.1023/A:1018966204465).